IEEJ Journal of Industry Applications
Vol.15 No.3 pp.332–345 DOI: 10.1541/ieejjia.20250117

Paper

Noncausal State Estimation for Iterative Learning Control

Kentaro Tsurumoto[*a)] Student Member, Wataru Ohnishi[*] Senior Member
Takafumi Koseki[*] Fellow, Nard Strijbosch[**] Non-member
Tom Oomen[**,***] Non-member

(Manuscript received May 16, 2025, revised Oct. 16, 2025)
J-STAGE Advance published date : Nov. 28, 2025

Next-generation high-precision mechatronic systems require safe and precise control of unmeasurable states. State-tracking iterative learning control (ILC) can achieve extremely high state-tracking performance up to the performance of state estimation, with convergence guaranteed apriori through the frequency-domain characteristics of the state estimator. The aim of this study is to develop a noncausal state estimation framework with verifiable frequency-domain characteristics. In batch-operated systems such as ILC, the use of noncausal design leads to substantial performance improvements that surpass the fundamental limits of causal approaches. Furthermore, by analytically verifying the frequency-domain characteristics of the noncausal state estimator, the developed framework retains the benefit of guaranteeing convergence in ILC. The developed framework is validated both by simulation and experiment, confirming improved state-tracking with monotonic convergence of ILC, achieved by exploiting noncausality in state estimation.

Keywords: state estimation, kalman smoother, fixed-interval smoother, iterative learning control, frequency-domain design

1. Introduction

Due to Moore's law, increasingly stringent performance requirements are posed for next-generation high-precision mechatronic systems[(1)]. This necessitates the consideration of trivial phenomena neglected in tradition motion control, e.g., internal deformation[(2)–(4)], unknown disturbances[(5)–(7)], continuous-time performance[(8)–(10)], which motivates the concept of controlling such unmeasurable phenomena by introducing additional state variables. Such utilization of state variables are introduced in the following examples.

A first example arises in an inferential control setup[(11)], where internal deformation and unknown disturbances between the point-of-interest (performance variable) and the sensor position (measured variable) must be explicitly considered[(12)]. Due to the performance variables not being directly accessible in real-time due to practical limitations or cost considerations[(13)], it is highly motivated to obtain accurate estimates, either online or offline, for improved tracking-performance.

A second example arises in a sampled-data system setup[(14)], where the controllers are implemented in discrete-time, but the tracking-performance of interest is in continuous-time. Enhanced tracking in continuous-time can be achieved by utilizing multirate inversion[(8)(9)(15)], where the aim is not only to achieve perfect-tracking for measured positions, but also the desired states in controllable canonical form, e.g., velocity, acceleration, jerk.

Iterative learning control[(16)(17)] (ILC) can significantly improve the control performance of systems performing repetitive tasks by utilizing experimental data from previous repeating iterations. In addition to its high tracking capability, with frequency-domain ILC, monotonic convergence can be ensured using frequency response functions (FRFs). This enabled frequency-domain ILC to be widely applied to various high-precision mechatronic systems, such as wafer stages[(18)], machine tools[(19)], atomic force microscopes[(20)(21)] and industrial printers[(22)].

The idea of utilizing ILC for tracking unmeasurable states has seen several developments in the past[(13)(23)(24)]. However, only the use of causal state estimators has been considered, e.g., Kalman filters[(25)] and state observers[(26)]. While nonlinear approaches performing beyond linear observers have been reported[(27)], in general, causal state estimators have a trade-off between estimation speed and noise sensitivity[(28)(29)]. Thus, the user is required to find a desirable balance. In ILC, the system is controlled batch-by-batch, allowing the use of noncausal filtering during offline optimization[(17)]. In such a situation, state estimation can be fundamentally improved by fixed-interval smoothing[(30)–(32)], which is essentially equivalent to a noncausal linear time-varying (LTV) filtering method.

Although fixed-interval smoothing can fundamentally improve ILC for tracking unmeasurable states compared to

a) Correspondence to: Kentaro Tsurumoto. E-mail: k.tsurumoto@ctl.t.u-tokyo.ac.jp
* Department of Electrical Engineering and Information Systems, The University of Tokyo
7-3-1, Hongo, Bunkyo-ku, Tokyo 113-8656, Japan
** Department of Mechanical Engineering, Eindhoven University of Technology
Eindhoven, Netherlands
*** Delft Center for Systems and Control, Delft University of Technology
Delft, Netherlands

using causal state estimations, frequency-domain characteristics of the estimator must be analyzable for ensuring monotonic convergence of frequency-domain ILC. The aim of this study is to: 1) develop a linear time-invariant (LTI) fixed-interval smoothing framework, suitable for analyzing the frequency-domain characteristics and implementation in ILC to ensure convergence; and 2) utilize noncausal state estimation for improving the state-tracking performance of ILC. Note that with LTI fixed-interval smoothing, the optimality of estimation is lost in cost of the frequency-domain interpretability.

The main contributions of this study are summarized as follows.

C1 Steady-state behavior of the LTV fixed-interval smoother is analyzed and an LTI model is developed (Section 3.3 and 3.4), applicable for ensuring convergence of state-tracking ILC (Section 5).

C2 State-estimation improvements and suboptimality of the developed LTI fixed-interval smoother are validated by a simulation setup (Section 4).

C3 With the developed LTI fixed-interval smoother, performance and robustness improvement of state-tracking ILC is validated by an experimental setup (Section 5).

This study extends the preliminary results reported in study (33) and (34), coupled with additional derivation of the LTI fixed-interval smoother and analysis on the influence of measurement noise. In addition, the developed LTI fixed-interval smoother is applied to ILC successfully in an experimental setup, assuming multiple modeling conditions.

1.1 Notation

Let $H(z)$ denote a discrete-time linear time invariant (LTI) system where

$$H(z) \overset{z}{:=} \left(\begin{array}{c|c} A_H & B_H \\ \hline C_H & D_H \end{array}\right), \cdots\cdots\cdots\cdots\cdots\cdots\cdots\cdots (1)$$

denotes a state-space representation

$$x_H[k+1] = A_H x_H[k] + B_H u_H[k] + w[k], \cdots\cdots (2)$$
$$y_H[k] = C_H x_H[k] + D_H u_H[k] + v[k], \cdots\cdots\cdots\cdots (3)$$

with state x_H having n variables, process noise w and measurement noise v being white, zero-mean, uncorrelated

$$w \sim \mathcal{N}(0, \sigma_w^2), \quad v \sim \mathcal{N}(0, \sigma_v^2), \cdots\cdots\cdots\cdots\cdots\cdots (4)$$

where σ_w^2 and σ_v^2 respectively denote covariance matrices of w and v. The transfer function is given by $H(z) = C_H(zI_{n\times n} - A_H)^{-1}B_H + D_H$ with $H(z) \in \mathcal{R}^{n_y \times n_u}$, where n_u and n_y respectively denote the dimension of input u_H and output y_H of the system. The frequency response function of $H(z)$ is obtained by substituting $z = e^{i\omega}\ \forall \omega \in [0, 2\pi)$, and is denoted by $H(e^{i\omega})$. The lengths of all signals are assumed to be $N \in \mathbb{N}$.

For a discrete-time signal x, the $k^{\text{th}} \in \mathbb{Z}$ time instance is expressed as $x[k]$, which corresponds to the continuous-time signal $x(kT_s)$ where T_s denotes the sampling time. The z-transform of signal $x[k]$ is specified as $x(z) = \sum_{k=-\infty}^{\infty} x[k]z^{-k}$.

Throughout this study (z) is omitted when obvious, $\hat{H}$ and $\hat{x}$ expressions are used to describe the estimation or model of system H and signal x, $\bar{\sigma}(\cdot)$ denotes the maximum singular value, and $I_{n\times n}$, $0_{n\times n}$ are $n \times n$ identity matrix and zero matrix. Furthermore, x_j denotes a signal for the j^{th} iteration number of the motion task, an aposteriori estimation of $x[k]$, i.e., estimation made using measurement data up to and including time instance k, is denoted by $\hat{x}^+[k]$, and the following notation is used for the analysis of lifted systems.

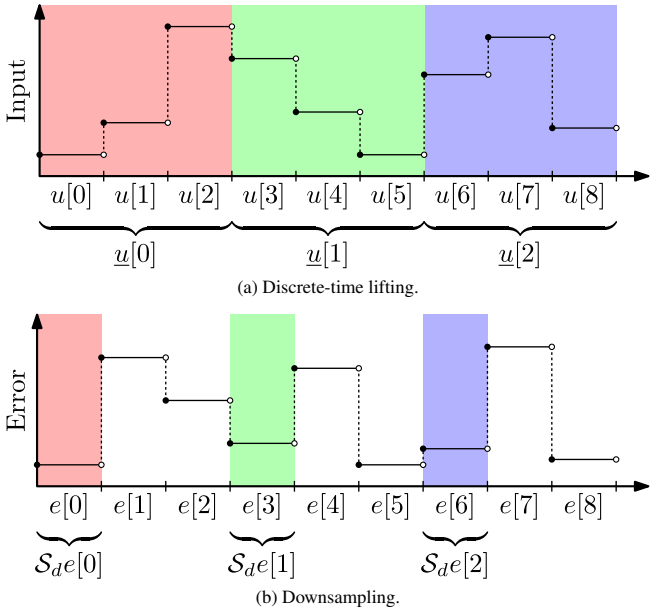

(a) Discrete-time lifting.
(b) Downsampling.

Fig. 1. Example of discrete-time lifting and downsampling for $\tau = 3$

Definition 1 (Discrete-time lifting) A lifted signal of $u[k]$ over $\tau \in \mathbb{N}$ samples is denoted by $\underline{u}[l] = \mathcal{L}u[k]$ with

$$\underline{u}[l] = \left[u[l\tau]^\top \ u[l\tau+1]^\top \ \cdots \ u[l\tau+\tau-1]^\top\right]^\top \in \mathbb{R}^\tau, \cdots\cdots\cdots\cdots\cdots (5)$$

where $l \in \mathbb{Z}$ and $\mathcal{L}$ denotes the lifting operator, which maps $u \mapsto \underline{u}$. An inverse lifting operator is given by $u = \mathcal{L}^{-1}\underline{u}$. An example of discrete-time lifting is illustrated in Figure 1(a). Lifting over τ sample multiplies the sampling period by $1/\tau$, and inverse lifting over τ sample multiplies the sampling period by τ.

Definition 2 (Lifted system in state space) The input/output of lifted system of H over τ samples would be $\underline{y} = \mathcal{L}y = (\mathcal{L}H\mathcal{L}^{-1})(\mathcal{L}u) = \underline{H}\underline{u}$. $\underline{H}$ can be obtained from a state-space model, and is denoted by

$$\underline{H} \overset{z^\tau}{=} \left(\begin{array}{c|c} \underline{A}_H & \underline{B}_H \\ \hline \underline{C}_H & \underline{D}_H \end{array}\right) \in \mathcal{R}^{\tau\times\tau} \cdots\cdots\cdots\cdots\cdots\cdots\cdots (6)$$

$$= \left(\begin{array}{c|ccc} A_H^\tau & A_H^{\tau-1}B_H & A_H^{\tau-2}B_H & \cdots & B_H \\ \hline C_H & D_H & 0 & \cdots & 0 \\ C_HA_H & C_HB_H & D_H & \cdots & 0 \\ \vdots & \vdots & \vdots & \ddots & \vdots \\ C_HA_H^{\tau-1} & C_HA_H^{\tau-2}B_H & C_HA_H^{\tau-3}B_H & \cdots & D_H \end{array}\right).$$

Definition 3 (Downsampling operator) The downsampling operation over τ samples is defined by

$$\mathcal{S}_d : \alpha[k] \mapsto \beta[k], \quad \beta[k] = \alpha[k\tau]. \cdots\cdots\cdots\cdots\cdots (7)$$

An example of downsampling is illustrated in Figure 1(b).

2. Problem Formulation

In this section the considered problem is defined by describing the system and introducing state-tracking ILC.

2.1 High-torque Direct-drive Motor

High-torque

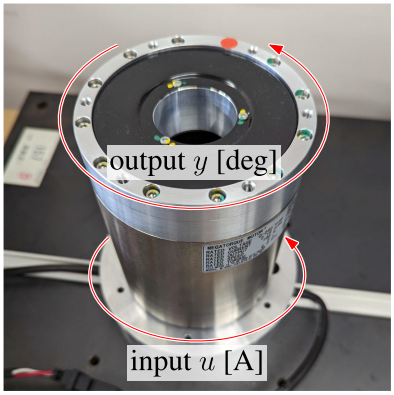

Fig. 2. High-torque direct-drive motor used for experimental validation

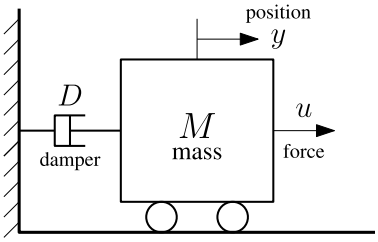

Fig. 3. Simulation model of a high-torque direct-drive motor used in Figure 2.

direct-drive motors deliver enhanced efficiency, precision, and versatility across a wide range of industrial applications.

In this study, methods are validated both in simulation and experimentally with a high-torque direct-drive motor shown in Figure 2. High-torque direct-drive motors can be modeled as a single-mass motion system as shown in Figure 3. In continuous-time, this system G_c is described as a second-order single-input-single-output system

$$G_c(s) = \frac{1}{Ms^2 + Ds} \overset{s}{=} \left(\begin{array}{cc|c} 0 & 1 & 0 \\ 0 & -D/M & 1/M \\ \hline 1 & 0 & 0 \end{array}\right), \quad \cdots\cdots (8)$$

assuming the controllable canonical form $x = [x_1, x_2]^\top = [y, \dot{y}]^\top$, where y denotes the motor angle degree. For this setup, coefficients of the system are $M = 3.1 \times 10^{-5}$ and $D = 2.6 \times 10^{-4}$, controlled at a sampling time T_s where the discrete-time system G is derived as

$$G(z) \overset{z}{=} \left(\begin{array}{c|c} e^{A_{G_c}T_s} & A_{G_c}^{-1}(e^{A_{G_c}T_s} - I_{2\times 2})B_{G_c} \\ \hline C_{G_c} & D_{G_c} \end{array}\right) \cdots\cdots (9)$$

2.2 System Description The control setup considered for this study is shown in Figure 4. Here, the continuous-time system G_c is discretized by a sampler and zero-order-hold as G. The discrete-time system G is controlled with a discrete-time system input $u[k]$, consisting of stabilizing discrete-time feedback controller K_{fb} and discrete-time feedforward input $f[k]$. Furthermore, $r[k]$ denotes the discrete-time reference sampled from the continuous-time reference $r(t)$, $y[k]$ the discrete-time system output sampled from the continuous-time output $y(t)$, $e[k]$ the discrete-time tracking-error sampled from the continuous-time error $e(t)$.

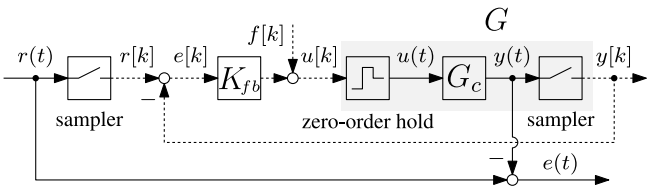

Fig. 4. Considered tracking-control configuration. The flow of the continuous-time signals are denoted by (→), whereas the discrete-time signals are denoted by (⇢). The objective of this study is to minimize the continuous-time error $e(t)$ with a discrete-time controller configuration

The considered control objective in this study is to minimize the continuous-time error $e(t)$, which includes both on-sample and inter-sample behavior, with a discrete-time control setup. For this study, the continuous-time reference $r(t)$ is assumed to be known in advance.

2.3 State-tracking ILC In this subsection, state-tracking ILC (ST-ILC) developed in study (24) is introduced.

The aim of ST-ILC is to learn the feedforward f_{j+1} achieving perfect state-tracking for a trial invariant state reference $r_x = r_{x,j+1} = r_{x,j} \in \mathbb{R}^n$. Generally in ILC, an FF input f_{j+1} which achieves perfect output-tracking, i.e., $r_{j+1} = y_{j+1}$, is learned using measurement data collected from previous iterations. In ST-ILC, this is modified to aim perfect state-tracking, i.e., $r_{x,j+1} = x_{j+1}$, by utilizing the concept of multirate inversion[8][9][15], designing the FF input $f_{j+1} = \mathcal{L}^{-1}\underline{f}_{j+1}$ as

$$\underline{f}_{j+1} = Q_x(\underline{f}_j + \alpha L_x \mathcal{S}_d \hat{e}_{x,j}), \cdots\cdots (10)$$

where $0 < \alpha \leq 1$ is the learning gain, $L_x \in \mathcal{R}^{n\times n}$ is the learning filter, $Q_x \in \mathcal{R}^{n\times n}$ is the robustness filter, and $\hat{e}_{x,j} \in \mathbb{R}^n$ is the estimated state-tracking error at the j^{th} iteration

$$\hat{e}_{x,j} = r_x - \hat{x}_j. \cdots\cdots (11)$$

Here the estimated state at the j^{th} iteration is obtained from

$$\hat{x}_j = O\begin{bmatrix} u_j^\top & y_j^\top \end{bmatrix}^\top, \cdots\cdots (12)$$

where $O \in \mathcal{R}^{n\times(n_u+n_y)}$ is the transfer function of the state estimator, and the system input and output at the j^{th} iteration are denoted by u_j and y_j. The update scheme of ST-ILC is illustrated in Figure 5. To facilitate the presentation, $\alpha = 1$ is assumed for this section. Smaller α can be exploited to mitigate the amplification of trial-varying disturbance at the cost of slower learning[35].

The estimate of state-tracking error $\mathcal{S}_d\hat{e}_{x,j}$ can be derived as

$$\mathcal{S}_d\hat{e}_{x,j} = S_{\hat{x}}\underline{r_x} - J_{\hat{x}}\underline{f}_j, \cdots\cdots (13)$$

where $S_{\hat{x}} \in \mathcal{R}^{n\times n^2}$ and $J_{\hat{x}} \in \mathcal{R}^{n\times n}$ respectively denote the sensitivity and process sensitivity of the state estimate. $S_{\hat{x}}$ and $J_{\hat{x}}$ are derived as

$$S_{\hat{x}} = \mathcal{S}\left(I_{n^2\times n^2} - \underline{G_{\hat{x}}K_{fb}S_y}\,\underline{C_G}\right), \cdots\cdots (14)$$

$$J_{\hat{x}} = \mathcal{S}\underline{G_{\hat{x}}S_u}, \cdots\cdots (15)$$

with system $G_{\hat{x}} \in \mathcal{R}^{n\times n_u}$, output and input sensitivity $S_y \in$

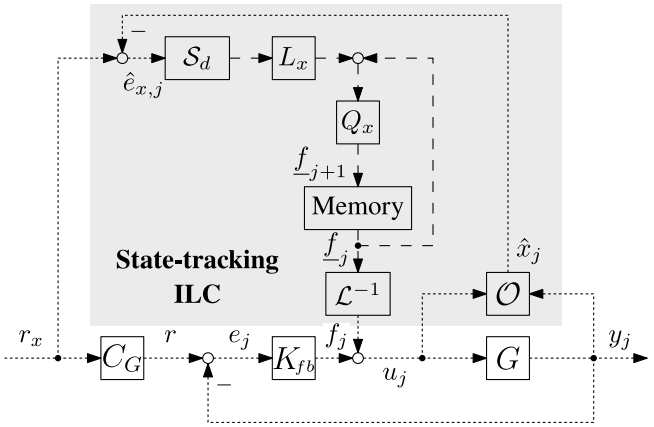

Fig. 5. Update scheme of state-tracking ILC, with j denoting the iteration number of the motion task. The flow of signals sampled by T_s are denoted by (-·►), whereas the slow-rate signals sampled by nT_s are denoted by (-►)

$\mathcal{R}^{n_y\times n_y}$ and $S_u \in \mathcal{R}^{n_u\times n_u}$, state selection matrix $\mathcal{S} \in \mathbb{R}^{n\times n^2}$ and lifted output matrix $\underline{C_G} \in \mathbb{R}^{n\times n^2}$

$$G_{\hat{x}} = O\begin{bmatrix} I_{n_u\times n_u} & G^\top \end{bmatrix}^\top,$$
$$S_y = (I_{n_y\times n_y} + GK_{fb})^{-1}, \quad S_u = (I_{n_u\times n_u} + K_{fb}G)^{-1},$$
$$\mathcal{S} = \begin{bmatrix} I_{n\times n} & 0_{n\times n(n-1)} \end{bmatrix}, \quad \underline{C_G} = I_{n\times n} \otimes C_G. \cdots\cdots (16)$$

Here $\otimes$ denotes the Kronecker tensor product. For further derivation of ST-ILC, see study (24).

From (10) and (13), it is guaranteed that $\|\underline{f}\|_2$ converges monotonically within the entire frequency domain ω when

$$\bar{\sigma}(Q_x(e^{i\omega})(I_{n\times n} - L_x(e^{i\omega})J_{\hat{x}}(e^{i\omega}))) < 1 \quad \forall\omega \in [0,\pi], \cdots\cdots (17)$$

is satisfied[36].

Remark 1 Similar to typical frequency-domain ILC, an advantage of ST-ILC is that nonparametric frequency response data of $J_{\hat{x}}$ can be used for testing learning convergence. This ensures monotonic convergence before executing the experiments.

When monotonic convergence condition (17) is satisfied, from (10) and (13), the asymptotic state-tracking error estimate $\lim_{j\to\infty} \mathcal{S}_d\hat{e}_{x,j} = \mathcal{S}_d\hat{e}_{x,\infty}$ and FF input $\lim_{j\to\infty} \underline{f}_j = \underline{f}_\infty$ are derived as

$$\mathcal{S}_d\hat{e}_{x,\infty} = \left(I_{n\times n} - J_{\hat{x}}(I_{n\times n} - Q_x(I_{n\times n} - L_xJ_{\hat{x}}))^{-1}Q_xL_x\right)S_{\hat{x}}\underline{r_x},$$
$$\underline{f}_\infty = (I_{n\times n} - Q_x(I_{n\times n} - L_xJ_{\hat{x}}))^{-1}Q_xL_xS_{\hat{x}}\underline{r_x}. \cdots\cdots (18)$$

Remark 2 When (17) is satisfied with $Q_x = I_{n\times n}$, the estimated states $\hat{x}_\infty$ perfectly track the desired state reference r_x for each n samples, i.e., $\mathcal{S}_d\hat{e}_{x,\infty} = 0$. In order for $Q_x = I_{n\times n}$ to be applicable, $\bar{\sigma}(I_{n\times n} - L_xJ_{\hat{x}}) < 1$ is required. This motivates the design of $L_x \approx J_{\hat{x}}^{-1}$.

Remark 3 As a cost of being limited to applications only performing a specific reference, convergence conditions for ILC frameworks are more relaxed compared to adaptive control schemes[37].

2.4 Problem Description While ST-ILC offers the benefit of potentially achieving perfect state-tracking performance, this comes with problems and limitations listed as follows.

- As addressed in Remark 2, ST-ILC can only ensure the estimated state $\hat{x}_\infty$ to achieve perfect state-tracking. Therefore, the actual tracking performance of ST-ILC is dependent on the quality of state estimation.
- For state estimator O in (12), previous studies only consider the use of causal state estimators, which have an inevitable trade-off between estimation speed and noise sensitivity.
- To ensure the convergence of ST-ILC from (17), frequency-domain characteristics of the state estimator O must be available. While LTI transfer functions for causal state estimators have been well developed[14], LTI transfer functions for noncausal state estimators have never been discussed.

In ST-ILC, state estimate $\hat{x}_j$ is only needed to calculate the update of FF input in (10). This permits the utilization of noncausal filtering, fundamentally improving the state estimation performance from causal filtering.

Hence, the problem addressed in this paper is to: 1) develop a noncausal LTI state estimation framework improving state-estimation performance compared to causal state estimators; 2) with frequency-domain characteristics available from the LTI model; and 3) apply it to ST-ILC for improved state-tracking performance with monotonic convergence.

3. Noncausal LTI Fixed-interval Smoother

In this section the LTI fixed-interval smoother is developed. First in Section 3.1, typical approaches for deriving the LTI transfer functions for causal state estimators are derived. Then in Section 3.2, a typical procedure of the noncausal LTV fixed-interval smoother is introduced. Finally, through a steady state analysis of the LTV fixed-interval smoother in Section 3.3, the transfer function of the developed LTI fixed-interval smoother is derived in Section 3.4. Section 3.3 and 3.4 constitute Contribution C1.

3.1 Steady-state Analysis of Causal Kalman Filter The optimal apriori state estimate $\hat{x}$ and aposteriori state estimate $\hat{x}^+$ of Kalman filter are given by computing the following equations

$$\hat{x}[k] = A_G\hat{x}^+[k-1] + B_Gu[k-1], \cdots\cdots (19)$$
$$\Sigma[k] = A_G\Sigma^+[k-1]A_G^\top + Q, \cdots\cdots (20)$$
$$K[k] = \Sigma[k]C_G^\top(C_G\Sigma[k]C_G^\top + R)^{-1}, \cdots\cdots (21)$$
$$\hat{x}^+[k] = \hat{x}[k] + K[k](y[k] - C_G\hat{x}[k]), \cdots\cdots (22)$$
$$\Sigma^+[k] = (I_{n\times n} - K[k]C_G)\Sigma[k]. \cdots\cdots (23)$$

for each time instance $k = 1, 2, \ldots, N$, with $Q \in \mathbb{R}^{n\times n}$, $R \in \mathbb{R}^{n_y\times n_y}$, $\hat{x}^+[0]$ and $\Sigma^+[0]$ initialized by the user[25][32]. Here, Σ and Σ^+ are covariances of $\hat{x}$ and $\hat{x}^+$, and K denotes the Kalman gain.

For detectable and stabilizable LTI systems, Kalman gain K and covariances Σ, Σ^+ converge to a steady-state[32] derived as

$$\Sigma[\infty] = A_G\Sigma[\infty]A_G^\top + Q \cdots\cdots (24)$$
$$-(A_G\Sigma[\infty]C_G^\top)(C_G\Sigma[\infty]C_G^\top + R)^{-1}(A_G\Sigma[\infty]C_G^\top)^\top,$$

$$K[\infty] = \Sigma[\infty]C_G^\top(C_G\Sigma[\infty]C_G^\top + R)^{-1}, \cdots\cdots\cdots (25)$$
$$\Sigma^+[\infty] = (I_{n\times n} - K[\infty]C_G)\Sigma[\infty], \cdots\cdots\cdots\cdots (26)$$

where (24) is the positive-semidefinite solution of the discrete-time algebraic Riccati equation. In steady-state Kalman filter, $K[k]$ in (21) and $\Sigma[k]$ in (23) are replaced with the steady-state $K[\infty]$ and $\Sigma[\infty]$. This results in a state estimate with a time-invariant update procedure reformulated as

$$\hat{x}[k] = A_G\hat{x}[k-1] + B_G u[k-1] + H(y[k-1] - C_G\hat{x}[k-1]), \cdots\cdots\cdots\cdots (27)$$
$$H = A_G K[\infty], \cdots\cdots\cdots\cdots\cdots\cdots\cdots\cdots (28)$$

where H is the static observer gain, resembling the Luenberger observer[26]. From (27), the transfer function of steady-state Kalman filter is derived as

$$O \overset{z}{=} \left(\begin{array}{c|cc} A_G - HC_G & B_G & H \\ \hline I_{n\times n} & 0_{n\times n_u} & 0_{n\times n_y} \end{array}\right), \cdots\cdots\cdots\cdots (29)$$

with the input being $[u^\top,\ y^\top]^\top$ and output being $\hat{x}$.

Remark 4 Although the steady-state Kalman filter is not optimal, its performance is indistinguishable from the optimal LTV Kalman filter for many practical problems[32]. With steady-state Kalman filter being LTI, it can be coupled with various frequency-domain analysis, which is fundamental for linear control theory.

3.2 Fixed-interval Smoothing When measurement data are accumulated after the k^{th} time instance, state estimations can be improved by Kalman smoothing[32]. Especially, smoothing for scenarios after the accumulation of full N time instances of measurement data is called fixed-interval smoothing[30][31].

In fixed-interval smoothing, all measurement data are utilized to obtain a smoothed estimate $\hat{x}_{sm}^{\text{LTV}}[k]$ by combining two optimal estimates $\hat{x}^+[k]$ and $\hat{x}_b[k]$, which are independent of each other. Here, $\hat{x}_b[k]$ is the optimal backward estimate, which can be interpreted as an apriori estimate of a Kalman filter (designed based on the inverted system dynamics) using measurement data from time instances $N, N-1, \ldots, k+1$. The concept of fixed-interval smoothing is illustrated in Figure 6.

The optimal backward estimate $\hat{x}_b[k]$ is given by computing the following equations

$$K_b[k] = \Sigma_b[k]C_G^\top(C_G\Sigma_b[k]C_G^\top + R)^{-1}, \cdots\cdots\cdots (30)$$
$$\hat{x}_b^+[k] = \hat{x}_b[k] + K_b[k](y[k] - C_G\hat{x}_b[k]), \cdots\cdots\cdots (31)$$
$$\Sigma_b^+[k] = (I_{n\times n} - K_b[k]C_G)\Sigma_b[k], \cdots\cdots\cdots\cdots (32)$$
$$\hat{x}_b[k-1] = A_G^{-1}(\hat{x}_b^+[k] - B_G u[k-1]), \cdots\cdots\cdots (33)$$
$$\Sigma_b[k-1] = A_G^{-1}\Sigma_b^+[k]A_G^{-\top} + A_G^{-1}QA_G^{-\top}, \cdots\cdots\cdots (34)$$

for each time instances $k = N, N-1, \ldots, 1$, with $\hat{x}_b[N] = 0$ and $\Sigma_b[N]$ initialized as a sufficiently large value[31][32]. Here, Σ_b and Σ_b^+ are covariances of $\hat{x}_b$ and $\hat{x}_b^+$, and K_b denotes the Kalman gain of backward estimate. Note that Q and R are the same parameters as the Kalman filter designed to obtain the forward estimate.

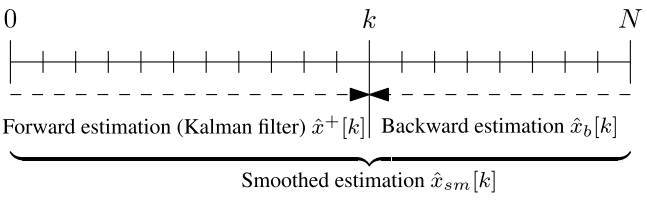

Fig. 6. Noncausal fixed-interval smoothng

In fixed-interval smoothing, an optimal smoothed estimate $\hat{x}_{sm}^{\text{LTV}}$ is obtained by a linear (time-varying) combination of $\hat{x}^+$ and $\hat{x}_b$ based on

$$\hat{x}_{sm}^{\text{LTV}}[k] = c_1[k]\hat{x}^+[k] + c_2[k]\hat{x}_b[k], \cdots\cdots\cdots\cdots (35)$$
$$c_1[k] = \Sigma_b[k](\Sigma^+[k] + \Sigma_b[k])^{-1}, \cdots\cdots\cdots\cdots (36)$$
$$c_2[k] = \Sigma^+[k](\Sigma^+[k] + \Sigma_b[k])^{-1}, \cdots\cdots\cdots\cdots (37)$$

where c_1 and c_2 are optimal matrix coefficients determined from the covariance matrices Σ^+ and Σ_b[32]. From update (35), the covariance matrix Σ_{sm}^{LTV} of $\hat{x}_{sm}^{\text{LTV}}$ is derived as

$$\Sigma_{sm}^{\text{LTV}}[k] = ((\Sigma^+[k])^{-1} + (\Sigma_b[k])^{-1})^{-1}, \cdots\cdots\cdots\cdots (38)$$

which is smaller than Σ^+ and Σ_b, implying improved accuracy by smoothing[32].

3.3 Steady-state Analysis of Fixed-interval Smoothing Similar to $\Sigma[\infty]$ and $K[\infty]$ in (24) and (25), the steady-state covariance matrix $\Sigma_b[-\infty]$ and Kalman gain $K_b[-\infty]$ for the backward estimation can be derived from (30), (32) and (34) as

$$\Sigma_b[-\infty] = A_G^{-1}\Sigma_b[-\infty]A_G^{-\top} - (A_G^{-1}\Sigma_b[-\infty]C_G^\top)\cdots (39)$$
$$\times(C_G\Sigma_b[-\infty]C_G^\top + R)^{-1}(A_G^{-1}\Sigma_b[-\infty]C_G^\top)^\top + A_G^{-1}QA_G^{-\top},$$
$$K_b[-\infty] = \Sigma_b[-\infty]C_G^\top(C_G\Sigma_b[-\infty]C_G^\top + R)^{-1}, \cdots\cdots (40)$$

where (39) is the positive-semidefinite solution of the discrete-time algebraic Riccati equation.

Remark 5 The asymptotic $\Sigma_b[-\infty]$ and $K_b[-\infty]$ resemble the $\Sigma[\infty]$ and $K[\infty]$ of Kalman filter, where A_G and Q are respectively replaced by A_G^{-1} and $A_G^{-1}QA_G^{-\top}$.

By replacing $K_b[k]$ in (30) and $\Sigma_b[k]$ in (34) with the steady-state $K_b[-\infty]$ and $\Sigma_b[-\infty]$, the time-invariant update law is derived as

$$\hat{x}_b[k-1] = A_b\hat{x}_b[k] + B_b u[k-1] + H_b(y[k] - C_G\hat{x}_b[k]), \cdots\cdots\cdots\cdots (41)$$
$$A_b = A_G^{-1},\quad B_b = -A_G^{-1}B_G,\quad H_b = A_G^{-1}K_b[-\infty]. \cdots\cdots (42)$$

Hence, when fixed-interval smoother is in steady-state, the smoothed estimate $\hat{x}_{sm}^{\text{LTI}}$ in (35) is approximated as

$$\hat{x}_{sm}^{\text{LTI}}[k] = c_1^{\text{const}}\hat{x}^+[k] + c_2^{\text{const}}\hat{x}_b[k], \cdots\cdots\cdots\cdots (43)$$
$$c_1^{\text{const}} = \Sigma_b[-\infty](\Sigma^+[\infty] + \Sigma_b[-\infty])^{-1}, \cdots\cdots\cdots (44)$$
$$c_2^{\text{const}} = \Sigma^+[\infty](\Sigma^+[\infty] + \Sigma_b[-\infty])^{-1}, \cdots\cdots\cdots\cdots (45)$$

where

$$\hat{x}^+[k] = \hat{x}[k] + K[\infty](y[k] - C_G\hat{x}[k]), \cdots\cdots\cdots (46)$$
$$\Sigma^+[\infty] = (I_{n\times n} - K[\infty]C_G)\Sigma[\infty]. \cdots\cdots\cdots\cdots (47)$$

From the aforementioned steady-state analysis, the estimation procedure for the developed LTI fixed-interval smoother is summarized as in Procedure 1.

3.4 Transfer Function of LTI Fixed-interval Smoother For the derivation of the transfer function of noncausal LTI

Procedure 1 (Update procedure of developed LTI fixed-interval smoother).

(1) Perform an experiment and collect the entire N samples of input u and output y data.

(2) Do a forward estimate to obtain $\hat{x}^+$.

(a) Determine $K[\infty]$ *and* $\Sigma^+[\infty]$ *from (24), (25), (47), solving the discrete-time algebraic Riccati equation.*

(b) Obtain $\hat{x}^+$ *from (46), using* $\hat{x}$ *obtained from (27).*

(3) Do a backward estimate to obtain $\hat{x}_b$.

(a) Determine $K_b[-\infty]$ *and* $\Sigma_b[-\infty]$ *from (39) and (40), solving the discrete-time algebraic Riccati equation.*

(b) Obtain $\hat{x}_b$ *from (41).*

(4) Combine the estimates to obtain $\hat{x}^{\mathrm{LTI}}_{sm}$.

(a) Obtain $\hat{x}^{\mathrm{LTI}}_{sm}$ *from (43).*

smoother, the following Lemma 1 and Theorem 1 are derived.

Lemma 1 (Transfer function of LTI forward estimator) The transfer function of the LTI forward estimator O^+, where the system input is $[u^\top,\ y^\top]^\top$ and output is $\hat{x}^+$, is derived as

$$O^+ = (I_{n\times n} - K[\infty]C_G)O + K[\infty]\begin{bmatrix}0_{n_y\times n_u} & I_{n_y\times n_y}\end{bmatrix}. \quad \cdots\cdots (48)$$

Proof. From

$$\hat{x}(z) = O\left[u(z)^\top y(z)^\top\right]^\top, \quad \cdots\cdots (49)$$

$$y(z) = \begin{bmatrix}0_{n_y\times n_u} & I_{n_y\times n_y}\end{bmatrix}\left[u(z)^\top \quad y(z)^\top\right]^\top, \cdots\cdots (50)$$

(48) is derived, using the superposition principle with (46). □

Theorem 1 (Transfer function of LTI backward estimator) The transfer function of the LTI backward estimator O_b, where the system input is $[u^\top,\ y^\top]^\top$ and output is $\hat{x}_b$, is derived as

$$O_b \times \begin{bmatrix}I_{n_u\times n_u} & 0_{n_u\times n_y}\\ 0_{n_y\times n_u} & z^{-1}I_{n_y\times n_y}\end{bmatrix} \triangleq \cdots\cdots (51)$$

$$\left(\begin{array}{c|cc}(A_b - H_bC_G)^{-1} & -(A_b - H_bC_G)^{-1}B_b & -(A_b - H_bC_G)^{-1}H_b\\ \hline I_{n\times n} & 0_{n\times n_u} & 0_{n\times n_y}\end{array}\right).$$

Proof. Rearranging (41) in terms of a causal update law yields

$$\hat{x}_b[k+1] = (A_b - H_bC_G)^{-1} \cdots\cdots (52)$$
$$\times(\hat{x}_b[k] - \begin{bmatrix}B_b & H_b\end{bmatrix}\left[u[k]^\top \quad y[k+1]^\top\right]^\top).$$

Therefore, by taking the z-transform of (52),

$$\hat{x}_b(z) = -(zI_{n\times n} - (A_b - H_bC_G)^{-1})^{-1}(A_b - H_bC_G)^{-1}$$
$$\times\begin{bmatrix}B_b & H_b\end{bmatrix}\begin{bmatrix}I_{n_u\times n_u} & 0\\ 0 & zI_{n_y\times n_y}\end{bmatrix}\begin{bmatrix}u(z)\\ y(z)\end{bmatrix}, \cdots\cdots (53)$$

is derived, which is equivalent to (51). □

Remark 6 The LTI backward estimator O_b is noncausal and unstable in a standard time forward filtering sense, implying its inapplicability online, e.g., real-time feedback systems.

From Lemma 1 and Theorem 1, the transfer function of LTI fixed-interval smoother is derived as follows.

Corollary 1 (Transfer function of LTI fixed-interval smoother) The transfer function of the LTI fixed-interval smoother O_{sm}, where the system input is $[u^\top,\ y^\top]^\top$ and output is $\hat{x}^{\mathrm{LTI}}_{sm}$, is derived as

$$O_{sm} = c_1^{\mathrm{const}}O^+ + c_2^{\mathrm{const}}O_b, \cdots\cdots (54)$$

where c_1^{const}, c_2^{const} are matrix coefficients from (43).

Proof. The proof follows from using the superposition principle with (43). □

Using the transfer function above, the developed LTI fixed-interval smoother can be analyzed in frequency-domain. This is further utilized in Section 4 for analyzing the performance of state estimation results, and in Section 5 for assuring convergent learning in ST-ILC.

4. Offline State Estimation Examples

In this section, offline state estimation results of the developed LTI fixed-interval smoother are validated both in time-domain and frequency-domain. To investigate the effectiveness of the developed framework, estimation results are compared with the steady-state Kalman filter using unified conditions, without any additional information or measurement data of the system. This section constitutes Contribution C2.

4.1 System Setup In this simulation validation, a high-torque direct-drive motor described in Section 2.1 with sampling time $T_s = 1\,\mathrm{ms}$, process noise $w = 0$ and measurement noise $v \sim \mathcal{N}(0, 10^{-6})$ is assumed.

For this validation, an offline state estimation after the execution of an open-loop motion task simulation is assumed. The control input u for the motion task is given as Figure 7(a), which results in the measured output data y shown in Figure 7(b). The true states x_1 and x_2 during the simulation task are displayed respectively in Figure 7(c) and Figure 7(d). The aim of state estimation is to obtain an accurate estimate close to the true x, (which is often difficult to obtain in experimental setups,) using input u and measurement data y, which are previously collected.

State estimations are conducted by assuming two scenarios. The first scenario is when the system is insufficiently identified and there exists a modeling error in the damping coefficient. The second scenario is when the system parameters are sufficiently identified, but there exists an unknown input disturbance. For both scenarios, the effect of assuming additional fictitious noise is also investigated, which is a standard approach for dealing with modeling error[28][32].

Finally, suboptimality of the developed LTI fixed-interval smoother is considered, by comparing the estimation results with optimal LTV fixed-interval smoother.

4.2 Example 1: Estimation with Model Parameter Error For this scenario, the state estimation is based on a system model $\hat{G}$ where $\hat{M} = M$ and $\hat{D} = 1.1D$.

4.2.1 Time-domain Analysis The state estimation result with $Q = \mathrm{diag}(10^{-5}, 1)$ and $R = 10^{-6}$ is shown in Figure 8. The result demonstrates that the estimation of steady-state Kalman filter yields an estimation error especially apparent in the velocity x_2. Due to the modeling error in the damping coefficient, an estimation error proportional to the velocity profile (Figure 7(d)) occurs. With the developed LTI fixed-interval smoother, the estimation error is significantly mitigated with less noise. This is achieved by

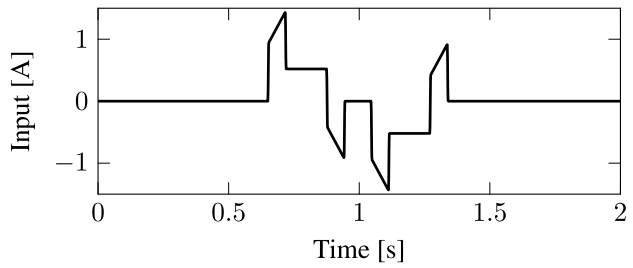

(a) Input current u.

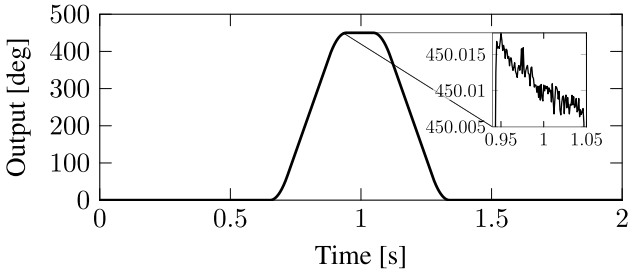

(b) Output position y with measurement noise.

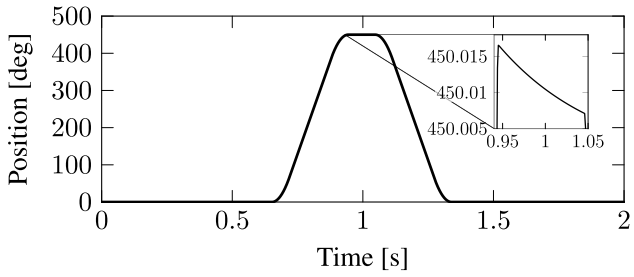

(c) True state $x_1 = y$.

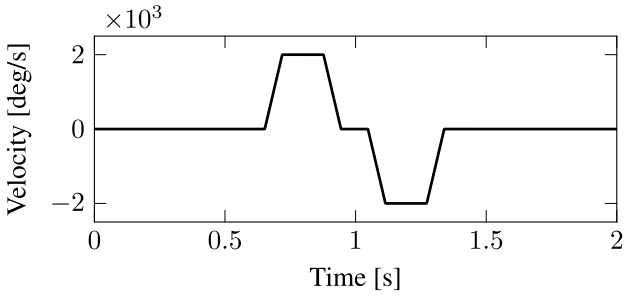

(d) True state $x_2 = \dot{y}$.

Fig. 7. Measurement data (a) and (b) used for offline state estimation, and validation data (c) and (d). These data are used for all Example 1, 2 and 3

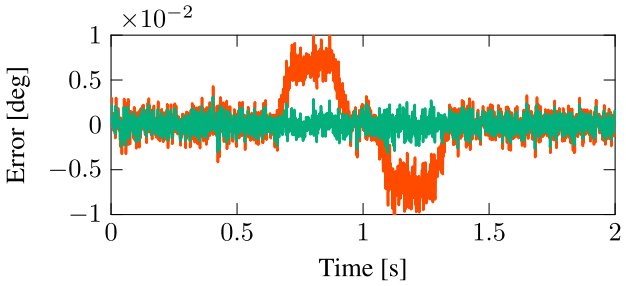

(a) State estimation error $x_1 - \hat{x}_1$.

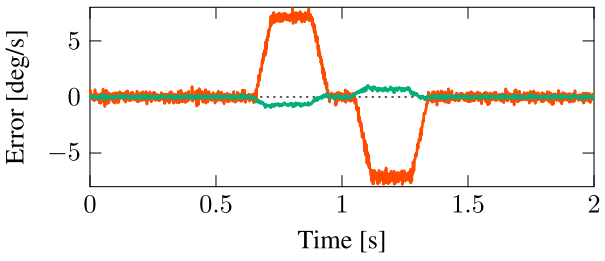

(b) State estimation error $x_2 - \hat{x}_2$.

Fig. 8. State estimation error of Example 1 with $Q = \mathrm{diag}(10^{-5}, 1)$ and $R = 10^{-6}$. State estimation results using the LTI fixed-interval smoother (—) outperform the causal steady-state Kalman filter (—) with less error amplitude and less noise amplification

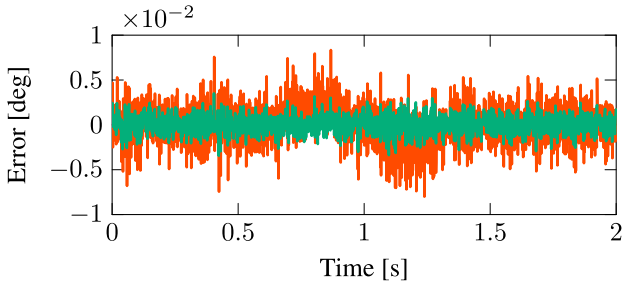

(a) State estimation error $x_1 - \hat{x}_1$.

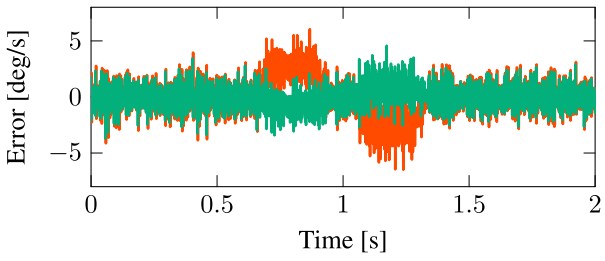

(b) State estimation error $x_2 - \hat{x}_2$.

Fig. 9. State estimation error of Example 1 with $Q = \mathrm{diag}(10^{-5}, 10^{2})$ and $R = 10^{-6}$. Compared to Figure 8, both causal steady-state Kalman filter (—) and LTI fixed-interval smoother (—), show either reduced or unchanged average error amplitude with significantly amplified noise

combining

(1) Forward estimation based on excessive damping assumption, leading to overestimation; with

(2) Backward estimation design on excessive damping assumption, but constructed using the inverted system dynamics as in (42), leading to underestimation,

resulting in minimization of modeling error and averaging out the effect of noise.

Figure 9 shows the result of state estimation assuming additional fictitious noise in x_2, designing $Q = \mathrm{diag}(10^{-5}, 10^{2})$. The result demonstrates that for steady-state Kalman filter, the magnitude of state estimation errors are decreased with the cost of amplified noise. An interesting observation is that with the LTI fixed-interval smoother, the estimation result does not improve, in fact, deteriorates due to noise amplification.

4.2.2 Frequency-domain Analysis For the frequency-domain analysis, let

- $G_{\hat{x}}$ denote the transfer function where the system input is $[u, y]^\top$ and output is $\hat{x}$, derived from (16) using O in

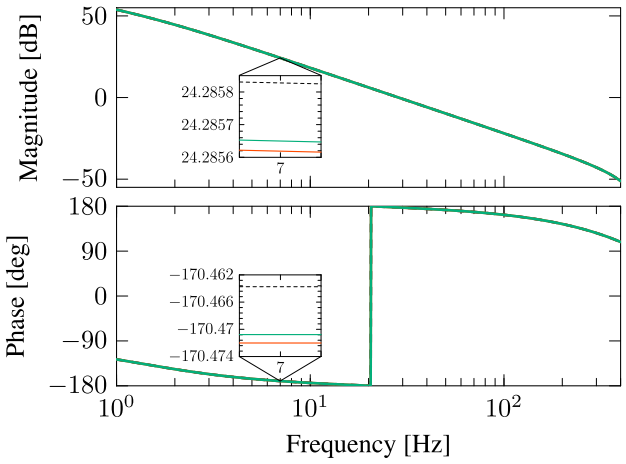

(a) input: u, output: x_1.

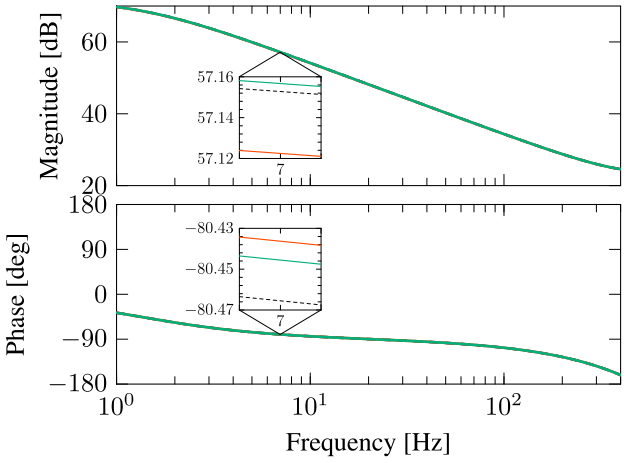

(b) input: u, output: x_2.

Fig. 10. Frequency-domain analysis of the state estimators designed in Example 1 with $Q = \mathrm{diag}(10^{-5}, 1)$ and $R = 10^{-6}$. Transfer function of the LTI fixed-interval smoother $G_{\hat{x}_{sm}^{\mathrm{LTI}}}$ (—) match the referred true system G_x (- - -) better, compared to the causal steady-state Kalman filter $G_{\hat{x}}$ (—)

(29).

- $G_{\hat{x}_{sm}^{\mathrm{LTI}}}$ denote the transfer function where the system input is $[u,\ y]^\top$ and output is $\hat{x}_{sm}^{\mathrm{LTI}}$, derived from (16) using O_{sm} in (54).
- G_x, with the subscript of the true state x, denote the transfer function where the system input is $[u,\ y]^\top$ and output is x, derived as, $G_x = (zI_{n\times n} - A_G)^{-1}B_G$.

In Figure 10, the Bode plot of the aforementioned transfer functions are shown. The result of the developed LTI fixed-interval smoother $G_{\hat{x}_{sm}^{\mathrm{LTI}}}$ matches the true response G_x more accurately compared to the steady-state Kalman filter $G_{\hat{x}}$. In addition, the gain difference between $G_{\hat{x}}$ and $G_{\hat{x}_{sm}^{\mathrm{LTI}}}$ is approximately 3×10^{-5} dB and 3.35×10^{-2} dB for x_1 and x_2, respectively. This indicates the improvement in state estimations x_1 and x_2, calculated from the velocity profile as 6.9×10^{-3} deg and 7.7 deg/s, respectively, approximately matching the estimation difference between $\hat{x}$ and $\hat{x}_{sm}^{\mathrm{LTI}}$ displayed in Figure 8.

4.3 Example 2: Estimation with Unknown Input Disturbance For this scenario, the state estimation is based

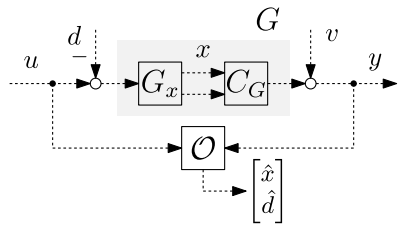

(a) Considered system with unknown input disturbance.

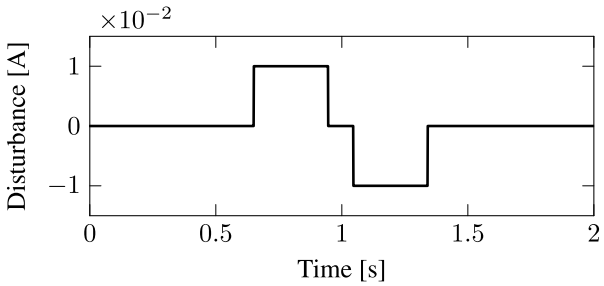

(b) Applied input disturbance d.

Fig. 11. Problem setup for Example 2 with unknown input disturbance

on a perfect system model $\hat{G}$ where $\hat{M} = M$ and $\hat{D} = D$, however, there is an unknown disturbance d. For the unknown disturbance, a simplified coulomb friction $d = 0.01\,\mathrm{sign}(\dot{y})$ is applied as an input disturbance, as shown in Figure 11. Slowly varying disturbance dynamics can be estimated by approximating the dynamics as a constant[38], i.e., $d[k+1] = d[k]$, where the state equation is augmented[39][40] as

$$\begin{bmatrix} x[k+1] \\ d[k+1] \end{bmatrix} = \begin{bmatrix} A_G & -B_G \\ 0 & 1 \end{bmatrix} \begin{bmatrix} x[k] \\ d[k] \end{bmatrix} + \begin{bmatrix} B_G \\ 0 \end{bmatrix} u[k], \cdots\cdots \quad (55)$$

derived as a transfer function

$$G_{\mathrm{DOB}} \overset{z}{=} \left(\begin{array}{cc|c} A_G & -B_G & B_G \\ 0_{1\times2} & 1 & 0 \\ \hline C_G & 0 & D_G \end{array}\right), \cdots\cdots\cdots\cdots\cdots \quad (56)$$

with the input as u, output as y and state as $[x^\top,\ d]^\top$. By using the new matrices defined in (56), LTI fixed-interval smoother can be applied as in Example 1, to obtain time-domain state estimation results from Procedure 1 and frequency-domain characteristics from (54). To facilitate the presentation, the results of the unknown disturbance estimate $\hat{d}$ are focused for this scenario.

4.3.1 Time-domain Analysis The state estimation results with $Q = \mathrm{diag}(10^{-5}, 1, 10^{-6})$ and $R = 10^{-6}$ are shown in Figure 12. The result demonstrates that the estimation of steady-state Kalman filter yields an estimation delay, while the LTI fixed-interval smoother yields a significantly mitigated estimation delay with less noise. This is achieved by the

(1) Forward estimation with estimation delay; and

(2) Backward estimation with estimation advance

complementing the estimation phase error and averaging out the effect of noise.

Figure 14 shows the result of state estimation assuming additional fictitious noise in d, designing $Q = \mathrm{diag}(10^{-5}, 1, 10^{-4})$. The result demonstrates that for both

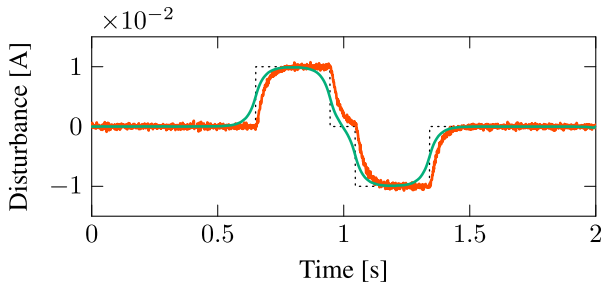

Fig. 12. Disturbance estimation of Example 2 with $Q = \mathrm{diag}(10^{-5}, 1, 10^{-6})$ and $R = 10^{-6}$. With the LTI fixed-interval smoother (—), estimation delay and the noise amplification are reduced compared to the steady-state Kalman filter (—)

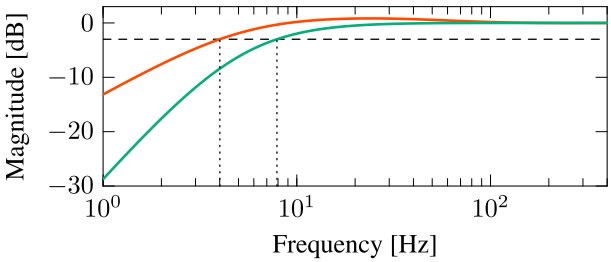

(a) input: d, output: $d - \hat{d}$.

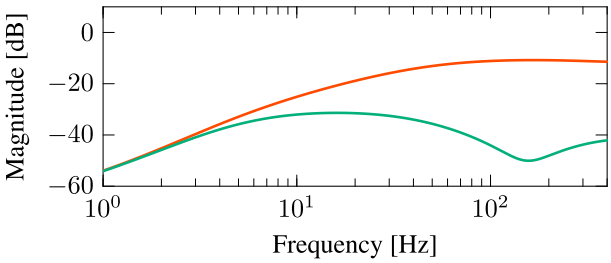

(b) input: v, output: $\hat{d}$.

Fig. 13. Frequency-domain analysis of the state estimators designed in Example 2 with $Q = \mathrm{diag}(10^{-5}, 1, 10^{-6})$ and $R = 10^{-6}$. Characteristics of the LTI fixed-interval smoother (—) discuss both the estimation error $d - \hat{d}$ and the noise amplification from v is reduced compared to the steady-state Kalman filter (—)

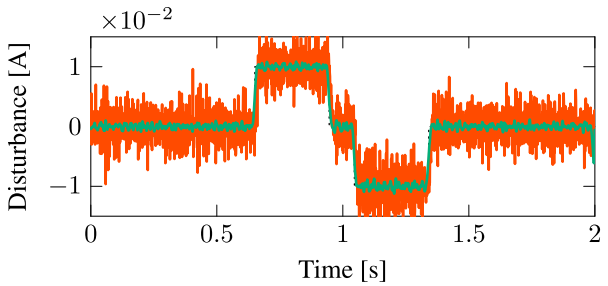

Fig. 14. Disturbance estimation of Example 2 with $Q = \mathrm{diag}(10^{-5}, 1, 10^{-4})$ and $R = 10^{-6}$. Compared to Figure 12, both the LTI fixed-interval smoother (—) and the steady-state Kalman filter (—) show reduced estimation delay with the cost of noise amplification

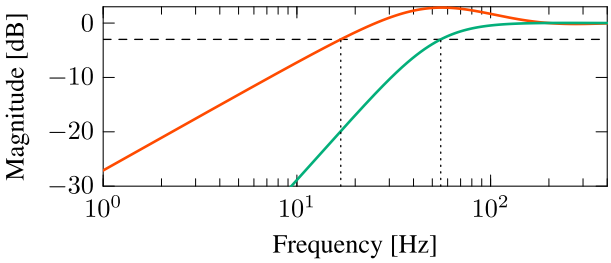

(a) input: d, output: $d - \hat{d}$.

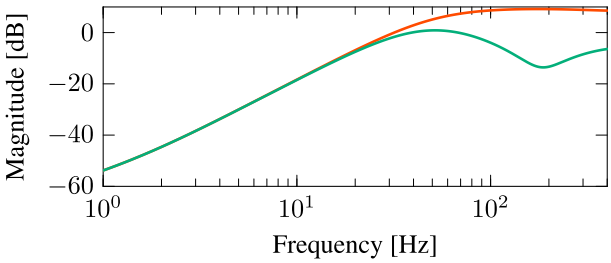

(b) input: v, output: $\hat{d}$.

Fig. 15. Frequency-domain analysis of the state estimators designed in Example 2 with $Q = \mathrm{diag}(10^{-5}, 1, 10^{-4})$ and $R = 10^{-6}$. Compared to Figure 13, the bandwidth of estimation error $d - \hat{d}$ is improved for both steady-state Kalman filter (—) and LTI fixed-interval smoother (—), with the cost of increased noise amplification from v

steady-state Kalman filter and noncausal LTI smoother, the estimation delay is mitigated with the cost of amplified noise. While the amplified noise severely deteriorates the estimation of steady-state Kalman filter, results show that the noise amplification for LTI fixed-interval smoother is not severe.

4.3.2 Frequency-domain Analysis To analyze the frequency-domain characteristics of estimation accuracy and noise amplification, let

- $S_{\hat{d}}$ denote the transfer function where the system input is d and output is $d - \hat{d}$, derived as,

$$S_{\hat{d}} = 1 - \begin{bmatrix} 0 & 0 & 1 \end{bmatrix} \mathcal{O} \begin{bmatrix} 0 & -G \end{bmatrix}^{\top} \cdots\cdots\cdots\cdots (57)$$

- $S_{\hat{d}^{\mathrm{LTI}}_{sm}}$ denote the transfer function where the system input is d and output is $d - \hat{d}^{\mathrm{LTI}}_{sm}$, derived similar as (57).

- $G_{\hat{d}v}$ denote the transfer function where the system input is v and output is $\hat{d}$, derived as

$$G_{\hat{d}v} = \begin{bmatrix} 0 & 0 & 1 \end{bmatrix} \mathcal{O} \begin{bmatrix} 0 & 1 \end{bmatrix}^{\top} \cdots\cdots\cdots\cdots\cdots (58)$$

- $G_{\hat{d}^{\mathrm{LTI}}_{sm}v}$ denote the transfer function where the system input is v and output is $\hat{d}^{\mathrm{LTI}}_{sm}$, derived similar as (58).

In Figure 13 and Figure 15, the Bode plot of the aforementioned transfer functions are shown, with Figure 13 showing the results of $Q = \mathrm{diag}(10^{-5}, 1, 10^{-6})$ and Figure 15 showing the results of $Q = \mathrm{diag}(10^{-5}, 1, 10^{-4})$. For both settings, it is observed that the bandwidth of the disturbance estimation is higher for the LTI fixed-interval smoother. This increased bandwidth leads to improved estimation results observed both in Figure 12 and Figure 14. In addition, from Figure 13(b) and Figure 15(b), it is observed that increasing the bandwidth of both estimators comes with the price of amplified noise. By increasing Q, the noise is amplified by about 20 dB for the steady-state Kalman filter, which is observed by comparing Figure 12 and Figure 14, where the magnitude of the noise is about 10 times larger. Additionally, $G_{\hat{d}^{\mathrm{LTI}}_{sm}v}$ for the higher bandwidth LTI fixed-interval smoother in Figure 15(b) is about the same as $G_{\hat{d}v}$ for the lower bandwidth steady-state Kalman filter in Figure 13(b). This is confirmed

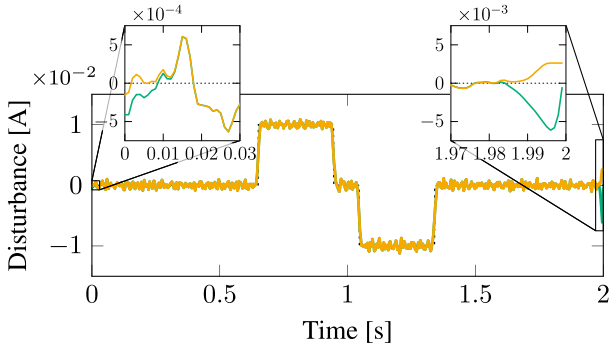

Fig. 16. Disturbance estimation with LTI (—) and LTV (—) fixed-interval smoother

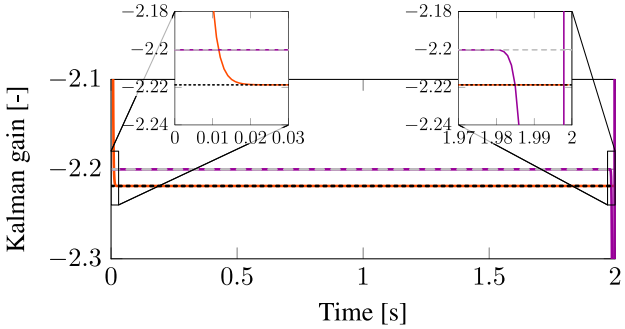

Fig. 17. Kalman gain K and K_b of LTI fixed-interval smoother (----, – –) and LTV fixed-interval smoother (—, —). After reaching steady-state, LTI and LTV fixed-interval smoother approaches the same value for both gains K and K_b

by comparing the noise level of $d - \hat{d}$ in Figure 12 and $d - \hat{d}_{sm}^{\mathrm{LTI}}$ in Figure 14. This indicates that the bandwidth of the LTI fixed-interval smoother is improved from 4 Hz to 55 Hz, without sacrificing the signal to noise ratio of estimation.

4.4 Example 3: Comparison with Optimal LTV Fixed-interval Smoother In Figure 16, the state estimation results of the optimal LTV fixed-interval smoother and suboptimal LTI fixed-interval smoother are shown. For the simulation setup, the design parameters in Example 2 (with $Q = \mathrm{diag}(10^{-5}, 1, 10^{-4})$) are used. From Figure 16, it is observed that: 1) during $t \in [0.02, 1.98]$, both LTV and LTI fixed-interval smoothers show identical estimation results; and 2) during $t \in [0, 0.02]$, $[1.98, 2]$, the LTV fixed-interval smoother shows better estimation results. This is interpretable from the time sequence of Kalman gain, displayed in Figure 17. From Figure 17, it is seen that during the transient period of forward estimation in $t \in [0, 0.02]$ and backward estimation in $t \in [1.98, 2]$, the Kalman gain of LTV fixed-interval smoother is adaptively adjusted. Due to the Kalman gain being optimally adjusted based on the covariance, this leads to improving the estimation of LTV fixed-interval smoother in Figure 16 during $t \in [0, 0.02]$, $[1.98, 2]$.

5. Application to ST-ILC

In this section, ST-ILC with the developed LTI fixed-interval smoother is experimentally validated with a high-torque direct-drive motor. To investigate the effectiveness of the developed framework, tracking results are compared with

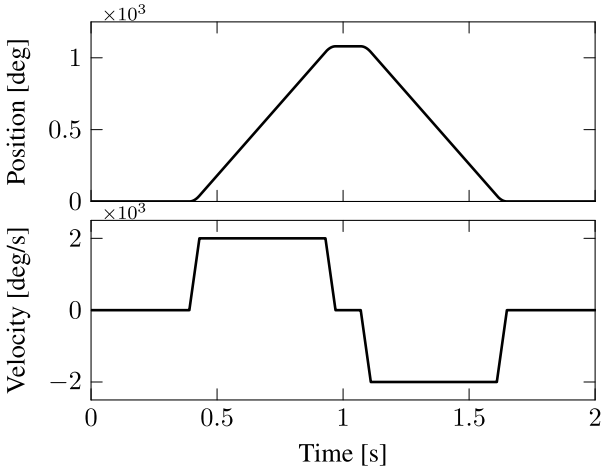

Fig. 18. State reference $r_x = [r, \dot{r}]^\top$ used for ST-ILC

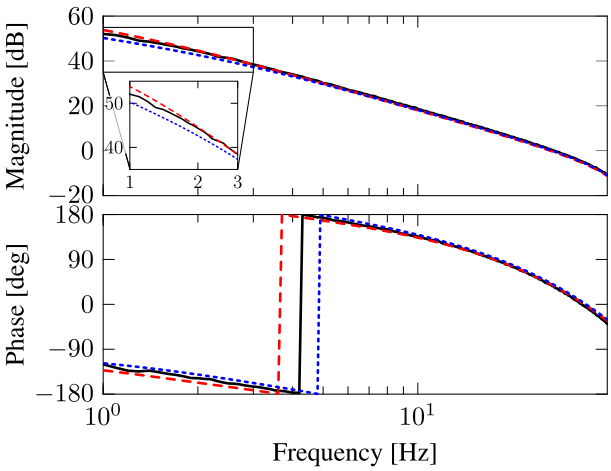

Fig. 19. Identified FRF of system (—) and sufficient model used for Case 1 (– –) and insufficient model used for Case 2 (----)

the conventional ST-ILC, which only uses causal steady-state Kalman filter. This section constitutes Contribution C3.

5.1 Experimental Setup In this experimental validation, a high-torque direct-drive motor described in Section 2.1 is controlled at a sampling time of $T_s = 10$ ms with a stabilizing FB controller

$$K_{fb}(z) = \frac{1.3837 \times 10^{-2}(1 - 0.8584 z^{-1})}{1 - 0.6327 z^{-1}} \cdots\cdots\cdots (59)$$

For this validation, the state reference shown in Figure 18 is assumed as the trial-invariant task and inter-sample data are collected every 1 ms. Note that the inter-sample data are only used for validation of $e(t)$ and not used for the control setup.

ST-ILC experiments are conducted assuming two scenarios. The first scenario is where the system is sufficiently identified and there is small modeling error, i.e., $\hat{M} \approx M$ and $\hat{D} \approx D$. The second scenario is where the system is insufficiently identified and there is a modeling error in the low frequency, i.e., $\hat{M} \approx M$ but $\hat{D} \approx 1.73D$. The FRF of the actual system G and model $\hat{G}$ used for Case 1 and 2 are shown in Figure 19. For both models of $\hat{G}$, the 1 sample delay measured from the FRF of G is also included.

For fair comparison in each case study, all state estimators

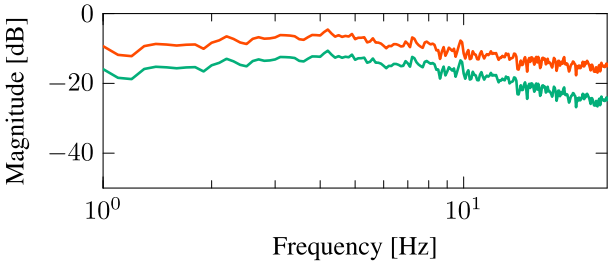

Fig. 20. Monotonic convergence condition of ST-ILC in Case 1 with sufficiently identified model. ST-ILC designed with the LTI fixed-interval smoother (—) show a larger margin from 0 dB compared to steady-state Kalman filter (—)

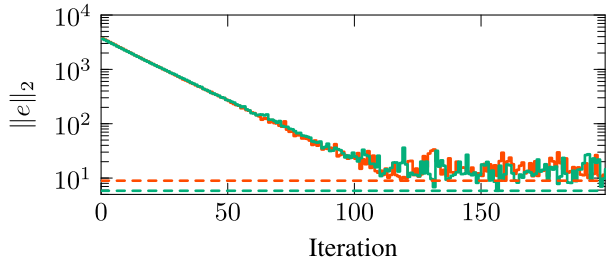

Fig. 21. Position error norm per iteration of ST-ILC in Case 1 with sufficiently identified model. Maximum tracking-performance achieved using the LTI fixed-interval smoother (—) outperforms the use of steady-state Kalman filter (—)

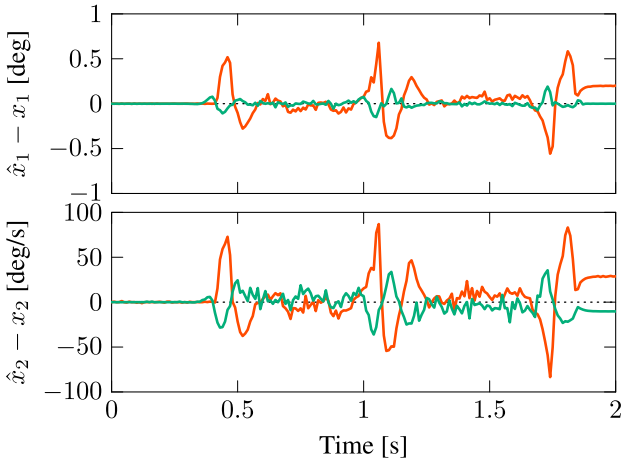

(a) State estimation error $\hat{x} - x$ (—) and $\hat{x}_{sm}^{\mathrm{LTI}} - x$ (—) at 1st iteration.

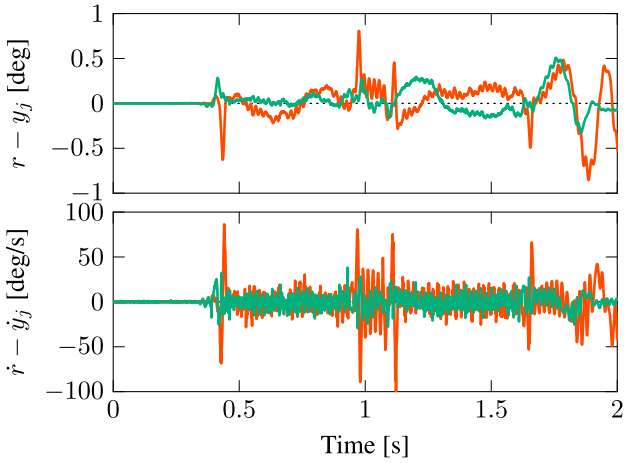

(b) State tracking error $r_x - x$ at best iteration, using steady-state Kalman filter (—) and LTI fixed-interval smoother (—).

Fig. 22. Experimental results of ST-ILC in Case 1 with sufficiently identified model

are designed with the same covariance matrix $Q = \mathrm{diag}(10^{-6}, 1)$ and $R = 10^{-6}$, learning settings with same learning gain $\alpha = 0.05$, robustness filter $Q_x = I_{n\times n}$ and learning filter $L_x = J_{\hat{x}}^{-1}$ calculated from model $\hat{G}$. Note that a low learning gain is set purely for validation purposes, to remove the influence of trial-varying noise and focus on the performance solely achieved by the methods[35].

5.2 Case 1: Performance with Sufficiently Identified Model For this scenario, all state estimations and learning are based on a system model $\hat{G}$ where $\hat{M} \approx M$ and $\hat{D} \approx D$.

First, Figure 20 shows the comparison of the monotonic convergence condition of ST-ILC derived from (17). Note that this is derivable for the LTI fixed-interval smoother using the transfer function developed in (54). The result shows that ST-ILC utilizing the LTI fixed-interval smoother exhibits a smaller maximum singular value, indicating enhanced robustness in learning. This is interpretable from the simulation results in the previous section, namely Figure 10. With the transfer function $G_{\hat{x}_{sm}^{\mathrm{LTI}}}$ being closer to the actual system G_x. This mitigates the imbalance between learning filter L_x and inverse process sensitivity $J_{\hat{x}}^{-1}$, resulting to a smaller $\bar{\sigma}(I_{n\times n} - L_x J_{\hat{x}})$.

Second, Figure 21 shows the norm of the inter-sample error $e(t) = r(t) - y(t)$ per iteration. Results show that the best performing error norm $\|e(t)\|_2$ with ST-ILC using the LTI fixed-interval smoother is reduced by 35% compared to that with the steady-state Kalman filter. Figure 22 shows the state-tracking results in the best performing iterations. With LTI fixed-interval smoother improving state estimation performance as in Figure 22(a), the peek tracking error of ST-ILC is mitigated for all states as shown in Figure 22(b). Moreover, the results show that state-tracking performance of ST-ILC can be indicated from state-estimation results of the 1st iteration.

Note that for this scenario with sufficient modeling, state estimation performance using the steady-state Kalman filter is sufficient enough. Therefore, after ST-ILC converges after 100 iterations, the bottleneck of the tracking-error becomes trial-varying noise. This results in identical average performance between both ST-ILC implementations using the LTI fixed-interval smoother and steady-state Kalman filter, as depicted in Figure 21.

5.3 Case 2: Performance with Insufficiently Identified Model For this scenario, all state estimations and learning are based on a system model $\hat{G}$ where $\hat{M} \approx M$ and $\hat{D} \approx 1.73D$.

First, Figure 23 shows the comparison of the monotonic convergence condition of ST-ILC derived from (17). Similar to Case 1 with sufficient modeling, the result shows that ST-ILC utilizing the LTI fixed-interval smoother exhibits a smaller maximum singular value, indicating enhanced robustness in learning. Compared to Figure 20, learning is less robust due to larger modeling error.

Second, Figure 24 shows the norm of the inter-sample

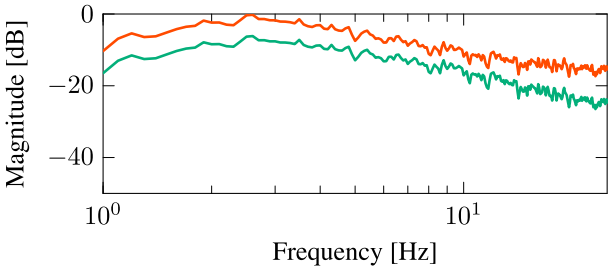

Fig. 23. Monotonic convergence condition of ST-ILC in Case 2 with insufficiently identified model. Similarly to Case1, ST-ILC designed with the LTI fixed-interval smoother (—) have a larger margin from 0 dB compared to steady-state Kalman filter (—)

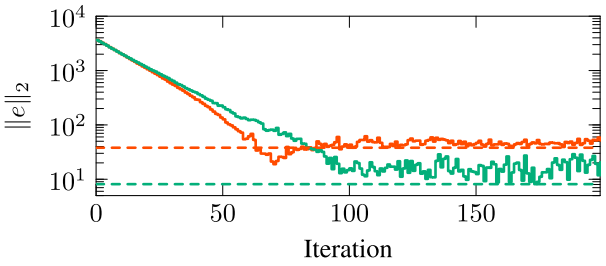

Fig. 24. Position error norm per iteration of ST-ILC in Case 2 with insufficiently identified model. Similarly to Case1, maximum tracking-performance achieved using the LTI fixed-interval smoother (—) outperforms the use of steady-state Kalman filter (—)

error $e(t) = r(t) - y(t)$ per iteration. Results show that the best performing error norm $\|e(t)\|_2$ with the fixed-interval smoother is reduced by 79% compared to that with the Kalman filter. Figure 25 shows the state-tracking results in the best performing iterations. Similarly to Case 1 with sufficient modeling, improved state estimation with the LTI fixed-interval smoother in Figure 25(a) leads to mitigated state-tracking error in Figure 25(b) when applied to ST-ILC. For this scenario with insufficient modeling, state estimation performance using the steady-state Kalman filter is insufficient. Therefore, after ST-ILC converges after 100 iterations, the bottleneck of the tracking-error becomes state-estimation error. This results in an apparent difference in average performance between both ST-ILC implementations using the LTI fixed-interval smoother and steady-state Kalman filter, as depicted in Figure 24.

Interestingly, from Figure 24, the error norm with the Kalman filter reaches a lower value before convergence. This is due to the state estimation of Kalman filter having an excessive gain with $\hat{D} \approx 1.73D$, which amplifies the effect of error used for learning. For this scenario, this modeling error has accelerated the learning in a positive manner. However, for other scenarios with deficient gain, decelerated learning leading to poor results is expected.

6. Conclusion

In this study, the developed LTI fixed-interval smoother fundamentally enhances the state-estimation performance, taking advantage of the batch-wise operation of ILC. This is successfully validated in simulation results analyzed both in time-domain and frequency-domain, assuming various

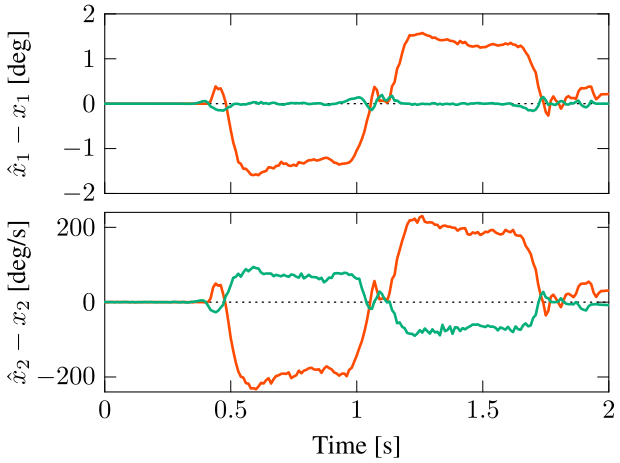

(a) State estimation error $\hat{x} - x$ (—) and $\hat{x}_{sm}^{\mathrm{LTI}} - x$ (—) at 1st iteration.

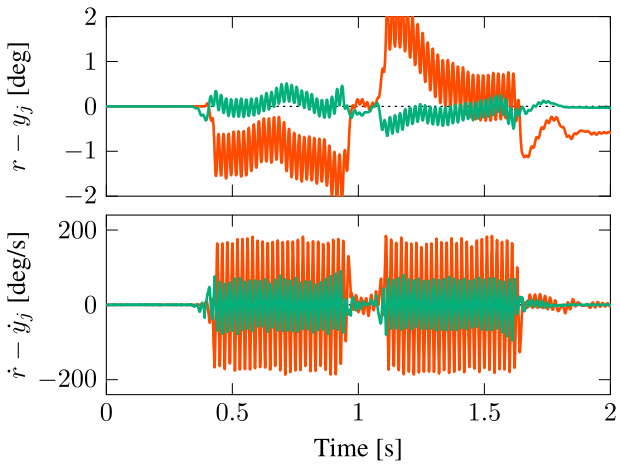

(b) State tracking error $r_x - x$ at best iteration, using steady-state Kalman filter (—) and LTI fixed-interval smoother (—).

Fig. 25. Experimental results of ST-ILC in Case 2 with insufficiently identified model

conditions of modeling error. Improved state-estimation directly contributes to improved state-tracking performance in ST-ILC, which is verified experimentally with a high-torque direct-drive motor setup. In addition, the developed transfer function of the LTI fixed-interval smoother provides important measures for enhancing monotonic convergence of ST-ILC.

Ongoing research focuses on applying noncausal LTI Kalman smoothing for repetitive control.

Acknowledgment

This work is supported in part by JSPS Grant-in-Aid for Scientific Research (B) Program Number 23H01431 and in part by JSPS Grant-in-Aid for JSPS Fellows under Grant 24KJ0959.

References

(1) M. Steinbuch, T. Oomen, and H. Vermeulen: “Motion Control, Mechatronics Design, and Moore’s Law”, *IEEJ Journal of Industry Applications*, Vol.11, No.2, pp.245–255 (2022)

(2) T. Oomen, R. Van Herpen, S. Quist, M. Van De Wal, O. Bosgra, and M. Steinbuch: “Connecting system identification and robust control for next-generation motion control of a wafer stage”, *IEEE Transactions on Control Systems Technology*, Vol.22, No.1, pp.102–118 (2014)

(3) R. Voorhoeve, R. De Rozario, W. Aangenent, and T. Oomen: "Identifying Position-Dependent Mechanical Systems: A Modal Approach Applied to a Flexible Wafer Stage", *IEEE Transactions on Control Systems Technology*, Vol.29, No.1, pp.194–206 (2021)

(4) Y. Kato, S. Sakaino, and T. Tsuji: "Motion Planning for Cutting Flexible Objects Based on Contact State Recognition", *IEEJ Journal of Industry Applications*, Vol.12, No.4, pp.786–792 (2023)

(5) K. Ohishi, M. Nakao, K. Ohnishi, and K. Miyachi: "Microprocessor-Controlled DC Motor for Load-Insensitive Position Servo System", *IEEE Transactions on Industrial Electronics*, Vol.IE-34, No.1, pp.44–49 (1987)

(6) M. Hoogerkamp, R.R. Waiboer, J. Van Dijk, and R.G. Aarts: "Attenuation of disturbances introduced by dynamic links in precision motion systems using model-based observers", *Mechatronics*, Vol.24, No.6, pp.640–647 (2014)

(7) W.H. Chen, J. Yang, L. Guo, and S. Li: "Disturbance-Observer-Based Control and Related Methods—An Overview", *IEEE Transactions on Industrial Electronics*, Vol.63, No.2, pp.1083–1095 (2016)

(8) H. Fujimoto, Y. Hori, and A. Kawamura: "Perfect Tracking Control Based on Multirate Feedforward Control with Generalized Sampling Periods", *IEEE Transactions on Industrial Electronics*, Vol.48, No.3 (2001)

(9) W. Ohnishi, T. Beauduin, and H. Fujimoto: "Preactuated Multirate Feedforward Control for Independent Stable Inversion of Unstable Intrinsic and Discretization Zeros", *IEEE/ASME Transactions on Mechatronics*, Vol.24, No.2, pp.863–871 (2019)

(10) T. Oomen, J. van de Wijdeven, and O. Bosgra: "Suppressing intersample behavior in iterative learning control", *Automatica*, Vol.45, No.4, pp.981–988 (2009)

(11) T. Oomen, E. Grassens, and F. Hendriks: "Inferential Motion Control: Identification and Robust Control Framework for Positioning an Unmeasurable Point of Interest", *IEEE Transactions on Control Systems Technology*, Vol.23, No.4, pp.1602–1610 (2015)

(12) N. Dirkx, N. Mooren, and T. Oomen: "Suppressing non-collocated disturbances in inferential motion control: With application to a wafer stage", in Proceedings of the American Control Conference, pp.4333–4338 (2021)

(13) J. Bolder and T. Oomen: "Inferential Iterative Learning Control: A 2D-system approach", *Automatica*, Vol.71, pp.247–253 (2016)

(14) T. Chen and B.A. Francis, *Optimal Sampled-Data Control Systems*, London, Springer (1995)

(15) M. Mae, W. Ohnishi, and H. Fujimoto: "Multirate feedforward control with mode decomposition for intersample performance in multivariable motion systems", *Control Engineering Practice*, Vol.141, p.105694 (2023)

(16) S. Arimoto, S. Kawamura, and F. Miyazaki: "Bettering operation of dynamic systems by learning: A new control theory for servomechanism or mechatronics systems", in The 23rd IEEE Conference on Decision and Control, pp.1064–1069 (1984)

(17) A. Bristow, Douglas, M. Tharayil, and A.G. Andrew: "A survey of iterative learning control", *IEEE Control Systems Magazine*, Vol.26, No.3, pp.96–114 (2006)

(18) X. Fu, X. Yang, P. Zanchetta, Y. Liu, C. Ding, M. Tang, and Z. Chen: "Frequency-Domain Data-Driven Adaptive Iterative Learning Control Approach: With Application to Wafer Stage", *IEEE Transactions on Industrial Electronics*, Vol.68, No.10, pp.9309–9318 (2021)

(19) T. Hayashi, H. Fujimoto, Y. Isaoka, and Y. Terada: "Projection-based iterative learning control for ball-screw-driven stage with consideration of rolling friction compensation", *IEEJ Journal of Industry Applications*, Vol.9, No.2, pp.132–139 (2020)

(20) E. Csencsics, S. Ito, J. Schlarp, and G. Schitter: "System Integration and Control for 3D Scanning Laser Metrology", *IEEJ Journal of Industry Applications*, Vol.8, No.2, pp.207–217 (2019)

(21) N. Nikooienejad, M. Maroufi, and S.O.R. Moheimani: "Iterative Learning Control for Video-Rate Atomic Force Microscopy; Iterative Learning Control for Video-Rate Atomic Force Microscopy", *IEEE/ASME Transactions on Mechatronics*, Vol.26, No.4 (2021)

(22) L. Blanken and T. Oomen: "Multivariable Iterative Learning Control Design Procedures: From Decentralized to Centralized, Illustrated on an Industrial Printer", *IEEE Transactions on Control Systems Technology*, Vol.28, No.4, pp.1534–1541 (2020)

(23) J. Wallén, M. Norrlöf, and S. Gunnarsson: "A framework for analysis of observer-based ILC", *Asian Journal of Control*, Vol.13, No.1, pp.3–14 (2011)

(24) W. Ohnishi, N. Strijbosch, and T. Oomen: "State-Tracking Iterative Learning Control in Frequency Domain Design for Improved Intersample Behavior", *International Journal of Robust and Nonlinear Control*, Vol.33, No.7, pp.4009–4027 (2023)

(25) R.E. Kalman: "A new approach to linear filtering and prediction problems", *Transactions of the ASME-Journal of Basic Engineering*, Vol.82, pp.35–45 (1960)

(26) D.G. Luenberger: "An Introduction to Observers", *IEEE Transactions on Automatic Control*, Vol.16, No.6, pp.596–602 (1971)

(27) Y.W. Jeong and C.C. Chung: "Observer-based Robust Control: Its Application to Permanent Magnet Synchronous Motors", *IEEJ Journal of Industry Applications*, Vol.12, No.4, pp.575–587 (2023)

(28) A.H. Jazwinski: "Adaptive filtering", *Automatica*, Vol.5, No.4, pp.475–485 (1969)

(29) R. Voorhoeve, N. Dirkx, T. Melief, W. Aangenent, and T. Oomen: "Estimating structural deformations for inferential control: a disturbance observer approach", *IFAC-PapersOnLine*, Vol.49, No.21, pp.642–648 (2016)

(30) H.E. Rauch, F. Tung, and C.T. Striebel: "Maximum likelihood estimates of linear dynamic systems", *AIAA Journal*, Vol.3, No.8, pp.1445–1450 (1965)

(31) D.C. Fraser and J.E. Potter: "The Optimun Linear Smoother as a Combination of Two Optimum Linear Filters", *IEEE Transactions on Automatic Control*, Vol.14, No.4, pp.387–390 (1969)

(32) D. Simon: *Optimal state estimation: Kalman, H infinity, and nonlinear approaches*, John Wiley & Sons (2006)

(33) K. Tsurumoto, W. Ohnishi, T. Koseki, N. Strijbosch, and T. Oomen: "Improved state estimation by non-causal state observer", in 8th IEEJ International Workshop on Sensing, Actuation, Motion Control, and Optimization, pp.447–450 (2022)

(34) K. Tsurumoto, W. Ohnishi, T. Koseki, N. Strijbosch, and T. Oomen: "Non-Causal State Estimation for Improved State Tracking in Iterative Learning Control", *IFAC-PapersOnLine*, Vol.55, No.37, pp.7–12 (2022)

(35) T. Oomen and C.R. Rojas: "Sparse iterative learning control with application to a wafer stage: Achieving performance, resource efficiency, and task flexibility", *Mechatronics*, Vol.47, pp.134–147 (2017)

(36) M. Norrlöf and S. Gunnarsson: "Time and frequency domain convergence properties in iterative learning control", *International Journal of Control*, Vol.75, No.14, pp.1114–1126 (2002)

(37) N. Kawamura, S. Inoue, T. Zanma, K. Kondo, K. Kenta, K.Z. Liu, and M. Shibata: "Feedback Error Learning-Based Position Control in Position-Sensorless Positioning Servo Systems for IPMSMs", *IEEJ Journal of Industry Applications*, Vol.12, No.4, pp.816–825 (2023)

(38) L.B. Freidovich and H.K. Khalil: "Performance recovery of feedback-linearization-based designs", *IEEE Transactions on Automatic Control*, Vol.53, No.10, pp.2324–2334 (2008)

(39) C.D. Johnson: "Accommodation of External Disturbances in Linear Regulator and Servomechanism Problems", *IEEE Transactions on Automatic Control*, Vol.16, No.6, pp.635–644 (1971)

(40) J.S. Meditch and G.H. Hostetter: "Observers for systems with unknown and inaccessible inputs", in IEEE Conference on Decision and Control including the 12th Symposium on Adaptive Processes, IEEE (73 CHO 806-0 SMC), pp.120–124 (1973)

Kentaro Tsurumoto (Student Member) received the M.Sc. degree in Department of Electrical Engineering and Information Systems from The University of Tokyo, Japan, in 2024. He is currently pursuing a Ph.D. degree in the Department of Electrical Engineering and Information Systems, Graduate School of Engineering, The University of Tokyo. He is a recipient of the IEEJ Industry Applications Society Excellent Presentation Award (SAMCON 2022). He is a student member of IEEE. His research interests include high-precision motion control and learning control.

Wataru Ohnishi (Senior Member) received the B.E., M.S., and Ph.D. degrees from The University of Tokyo, Japan, in 2013, 2015, and 2018, respectively. He is currently an associate professor with the Department of Electrical Engineering and Information Systems, Graduate School of Engineering, The University of Tokyo. He held a visiting position at the Eindhoven University of Technology. He is a member of IEEE. His research interests include high-precision motion control and optimization.

Takafumi Koseki (Fellow) received his Ph.D. degree from The University of Tokyo, Japan, in 1992. He is currently a professor with the Department of Electrical Engineering and Information Systems, Graduate School of Engineering, The University of Tokyo. He is a member of IEEE, Japan Society of Mechanical Engineering, Japan Society of Applied Electromagnetics and Mechanics, Japan Society of Precision Engineering, Japan Railway Electrical Engineering Association. His research interests include public transport systems, particularly linear drives, and the analysis and control of traction systems.

Nard Strijbosch (Non-member) received his B.Sc. degree (cum laude), M.Sc. degree (cum laude) and Ph.D. degree from the Eindhoven University of Technology, Eindhoven, The Netherlands. He is currently a system engineer at IBS Precision Engineering. He is a recipient of the IEEJ Industry Applications Society Excellent Presentation Award (SAMCON 2018). His research interest is in the field of motion control and learning control techniques for applications in mechatronic systems.

Tom Oomen (Non-member) received the M.Sc. degree (cum laude) and Ph.D. degree from the Eindhoven University of Technology, Eindhoven, The Netherlands. He is currently a professor with the Department of Mechanical Engineering at the Eindhoven University of Technology. He is also a part-time full professor with the Delft University of Technology. He held visiting positions at KTH, Stockholm, Sweden, and at The University of Newcastle, Australia. He is a recipient of the 7th Grand Nagamori Award, the Corus Young Talent Graduation Award, the IFAC 2019 TC 4.2 Mechatronics Young Research Award, the 2015 IEEE Transactions on Control Systems Technology Outstanding Paper Award, the 2017 IFAC Mechatronics Best Paper Award, the 2019 IEEJ Journal of Industry Applications Best Paper Award, and recipient of a Veni and Vidi personal grant. He is Senior Editor of the IEEE Control Systems Letters (L-CSS) and Co-Editor-in-Chief of IFAC Mechatronics. He has also served as Associate Editor for IFAC Mechatronics, IEEE Transactions on Control Systems Technology, and IEEE Control Systems Letters (L-CSS). He is a member of the Eindhoven Young Academy of Engineering. His research interests are in the field of data-driven modeling, learning, and control, with applications in precision mechatronics.